Full length article

Effects of liquid water addition on turbulent premixed hydrogen/air combustion

Riccardo Concetti [a],*, Josef Hasslberger [a], Nilanjan Chakraborty [b], Markus Klein [a]

[a] *Department of Aerospace Engineering, University of the Bundeswehr Munich, Werner-Heisenberg-Weg 39, Neubiberg, 85577, Germany*
[b] *School of Engineering, Newcastle University, Stephenson Building Claremont Road, Newcastle-Upon-Tyne, NE1 7RU, United Kingdom*

ARTICLE INFO

ABSTRACT

Statistically planar premixed hydrogen/air flames with and without liquid water injection are numerically investigated through Direct Numerical Simulations. The approach used for studying the interaction of the liquid dispersed phase with the gaseous carrier phase is a hybrid Eulerian–Lagrangian scheme with two-way coupling. The results show that the water injection acts to attenuate the differential diffusion effects arising from non-unity Lewis number and thermal expansion effects, especially under stoichiometric conditions. Furthermore, the size effect of the water droplets is considered by comparing the simulation results for two different initial droplet diameters of the water mist. In a second series of simulations, the effect of preferential diffusion is analysed in isolation. In these cases, the fuel has the same properties as hydrogen but a unity Lewis number. It is observed that the combined action of preferential diffusion and turbulence-induced wrinkling acts to increase the turbulent burning velocity in the regime considered here, while flame thickening acts to decrease the turbulent flame area in the fuel-lean cases and as a consequence weakens the effectiveness of preferential diffusion effects.

1. Introduction

The technique of injecting liquid water inside internal combustion engines has already been implemented in the mid of last century (e.g. Pratt & Whitney J57 engine and 1962 Oldsmobile Jetfire). The idea was to increase the power output for short periods due to the increase of the overall mass flow within the combustion chamber. However, in recent years, the technique has been getting attention again due to other side effects not considered in the past, like the decrease of maximum combustion temperature and the related decrease of NO_x production and emission. Several recent numerical and experimental studies have demonstrated the effectiveness of this technique on the efficiency gain and reduction of emissions [1,2]. The study of the interaction of liquid water with turbulent flames is also of paramount importance for safety reasons, for example, in plant fire extinguishers [3]. The primary effects of liquid water interaction with flames include:

- Cooling: This arises from the extraction of heat due to phase change.
- Dilution: The increase in water vapour concentration results in a decrease in the concentrations of fuel and oxidizer.
- Chemical effects: Previous analysis [4,5] has highlighted how steam influences radical production and temperature distribution

within the flame, thereby altering its structure. Furthermore, water is a principal combustion product of many fuels and the injection of steam into the system modifies the thermo-chemical equilibrium state.

In this study, following [6], only the first two effects are considered, as the last one is deemed of secondary importance (for the present configurations), primarily due to the low concentration of steam resulting from droplet evaporation within the flame, as will be demonstrated later. The focus in recent years is also to reduce or eliminate carbon dioxide emissions. For this reason, much research is now directed towards the combustion of carbon-free fuels, and the most representative one is hydrogen. The challenge of hydrogen combustion is particularly critical when a fuel-lean mixture is considered where the effects related to preferential diffusion and intrinsic flame instabilities become significant, for example, the thermo-diffusive instability, can occur.

The strength of the thermo-diffusive effects increases with decreasing characteristic Lewis number, which represents the ratio of the thermal diffusivity to the mass diffusivity of the mixture, and the flame becomes unconditionally unstable below the critical Lewis number. A number of previous analytical [7–10], experimental [11–13]

and computational [14–23] studies focused on the effects of Lewis number on several aspects of premixed turbulent combustion. It has been found that the overall burning rate, rate of flame propagation and the extent of flame wrinkling increase with decreasing Lewis number. Moreover, the effects of thermal expansion and flame normal acceleration strengthen with decreasing Lewis number. This also leads to the augmentation of turbulent velocity fluctuations induced by thermal expansion in premixed flames with decreasing Lewis number. All of these analyses have been carried out for single-phase gaseous conventional turbulent premixed flames. In the literature, there are experimental studies on the effect of liquid water injection on flames with non-unity Lewis number [24,25]. Nevertheless, a detailed study of the effect of preferential diffusion and the local effects of water evaporation on the flame has not been carried out. Moreover, to date, the interaction of water droplets with premixed flames with non-unity characteristic Lewis number is yet to be numerically analysed in detail although this information is fundamental to the physical understanding of the effects of water injection on turbulent premixed H_2-air flames. The present work fills the aforementioned gap in the literature by carrying out Direct Numerical Simulations (DNS) of the interaction of water droplets with statistically planar premixed flames representing H_2-air combustion for different equivalence ratios, water loadings and initial water droplet diameters. Moreover, the effects of differential diffusion induced by non-unity Lewis number in hydrogen-air flames are identified in this analysis by comparing the water droplet-flame interaction between non-unity and unity Lewis number conditions. It is noteworthy to state that the simulations conducted in this study do not consider fuel-rich mixtures (i.e., $\phi > 1.0$). Fuel-rich H_2-air flames can be characterized by an effective Lewis number greater than unity. Such mixtures typically exhibit reduced flame speed enhancement and flame surface wrinkling as well as the absence of thermo-diffusive instabilities, potentially leading to less relevant operating conditions from an engineering perspective. Furthermore, in practical contexts such as gas turbines for power generation and the mitigation of accidental fire propagation, lean conditions are typically more relevant, and therefore, only fuel-lean H_2-air flames are considered in this paper.

In the following section, the mathematical background will be presented, before Section 3 will show the simulation results, and Section 4 will present the conclusions of the present study.

2. Mathematical background and numerical implementation

In this work, $3D$ direct numerical simulations of statistically planar premixed turbulent hydrogen/air flames with liquid water injection are performed. A finite-difference code SENGA+ is utilized for $3D$ compressible reacting flows. The spatial discretization is implemented through a high-order central-difference scheme, while the explicit time advancement is accomplished through a third-order low-storage Runge–Kutta method. The domain of the simulation is a parallelepiped of dimension $30\delta_{st} \times 20\delta_{st} \times 20\delta_{st}$ where δ_{st} is the thermal flame thickness of the stoichiometric mixture, defined as:

$$\delta_{st} = \frac{\hat{T}_{ad,(\phi=1)} - \hat{T}_0}{max|\nabla\hat{T}|_L} \qquad (1)$$

Here $\hat{T}_0$, $\hat{T}_{ad,(\phi=1)}$ and $\hat{T}$ are the unburned gas temperature, adiabatic flame temperature for the stoichiometric mixture and the instantaneous dimensional temperature, respectively, while $max|\nabla\hat{T}|_L$ refers to the maximum value of the magnitude of the temperature gradient under laminar conditions. A uniform Cartesian grid of dimension $384 \times 256 \times 256$ is used for the discretization of the computational domain, and it resolves δ_{st} using at least 10 points. The imposed boundary conditions are non-reflective inflow–outflow in the direction of mean flame propagation, and periodic in the transverse directions. The initial thermo-chemical fields are derived from a 1D laminar simulation employing the same chemical model, reactant concentrations, and unburned temperature $\hat{T}_0 = 300\ K$. Droplets are introduced

into the unburned gas region of the domain at random positions but with a homogeneous distribution to avoid any artificial clustering, and their initial temperature matches that of the unburned reactants. The introduced water mist consists of monodispersed droplets, with initial diameters of $a_d/\delta_{st} = 0.02$ or 0.04, corresponding to about $10 - 20\ \mu m$. These values are commonly encountered in experimental studies or technical applications documented in the literature [26–28]. A schematic representation of the configuration setup is provided in Fig. 1. This code and the present configuration have been used in several previous studies [6,29,30]. The simulation method considering the liquid and gaseous phases is a hybrid Eulerian–Lagrangian approach, and the interaction between the two phases is implemented through a two-way coupling. The liquid particles are tracked along their paths in the domain, and their evolution affects the gaseous transport equations through coupling terms. The governing equations for the liquid particles are the following:

$$\frac{d\vec{x}_d}{dt} = \vec{u}_d; \qquad \frac{d\vec{u}_d}{dt} = \frac{\vec{u}(\vec{x}_d,t) - \vec{u}_d}{\tau_d^u};$$

$$\frac{da_d^2}{dt} = -\frac{a_d^2}{\tau_d^p}; \qquad \frac{dT_d}{dt} = \frac{\hat{T}(\vec{x}_d,t) - T_d - B_d L_v/C_p^g}{\tau_d^T} \qquad (2)$$

$$\tau_d^u = \frac{\rho_d a_d^2}{18 C_u \mu}; \qquad \tau_d^p = \frac{\rho_d a_d^2}{4\mu}\frac{Sc}{Sh_c ln(1+B_d)};$$

$$\tau_d^T = \frac{\rho_d a_d^2}{6\mu}\frac{Pr}{Nu_c}\frac{B_d}{ln(1+B_d)}\frac{C_p^l}{C_p^g} \qquad (3)$$

Hence, equations are solved for the droplet position, velocity, temperature and diameter ($\vec{x}_d$, $\vec{u}_d$, T_d and a_d). Here, C_u is a drag coefficient correction computed from the relation $C_u = 1 + Re_d^{2/3}/6$, where the droplet Reynolds number Re_d is computed from the velocity difference between the droplets and the surrounding gas. In Eq. (3), Nu_c and Sh_c represent the corrected Nusselt and Sherwood numbers and are assumed to be identical. The Spalding number B_d is computed by considering the equilibrium gaseous water concentration at the interface using the Clausius–Clapeyron relation. The Prandtl and the Schmidt numbers, Pr and Sc, are taken to be 0.7. The gas phase balance equations can be expressed with the following general form:

$$\frac{\partial(\rho\varphi)}{\partial t} + \frac{\partial(\rho u_j \varphi)}{\partial x_j} = \frac{\partial}{\partial x_j}\left(R_\varphi \frac{\partial\varphi^*}{\partial x_j}\right) + \dot{\omega}_\varphi + \dot{S}_g + \dot{S}_\varphi \qquad (4)$$

where the variable φ represents $\varphi = \{1, u_i, e, Y_F, Y_O, Y_W^g\}$ and $\varphi^* = \{1, u_i, T, Y_F, Y_O, Y_W^g\}$, for the mass, momentum, energy, fuel, oxidizer and gaseous water rising from evaporation, respectively. The coefficient R_φ is the diffusion coefficient, $\dot{\omega}_\varphi$ is the chemical source term, and $\dot{S}_g$ is a general source/sink term. Finally, $\dot{S}_\varphi$ is the term that describes the coupling between the liquid and gaseous phases. The expression for this term is provided by the following equation:

$$\dot{S}_\varphi = -\frac{1}{V_{cell}}\sum \frac{d(m_d \varphi_d)}{dt} \qquad (5)$$

Here, the subscript d denotes quantities related to droplets, where the mass of each droplet (m_d) is calculated assuming it to be a sphere with uniform density and the diameter coming from the solution of Eq. (2), while V_{cell} is the volume defined by the grid resolution. The individual contributions from each droplet are distributed to neighbouring grid points via trilinear interpolation of the source term. Given that the droplets consist solely of water, there are no source terms in the fuel and oxidizer equations, and mass conservation is maintained by adjusting the mass fractions of non-transported species to ensure $\sum Y_k = 1$. More details on the methodology can be found in previous works [6,29,30].

In the present work, the chemistry description is based on a single-step irreversible reaction, where the reaction rate is described through a single-step Arrhenius type chemistry [31] with the pre-exponential factors adjusted in a manner that the normalized laminar burning velocity $S_{L,(\phi)}/S_{L,(\phi=1)}$ variation with equivalence ratio ϕ obtained
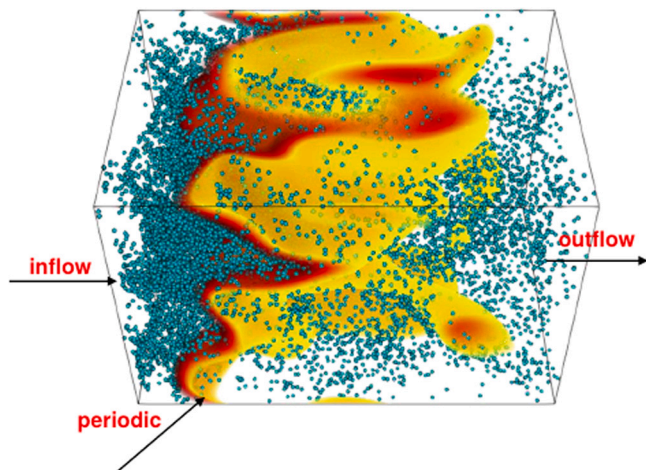
Fig. 1. Sketch of the computational domain and boundary conditions. The blue dots represent the water droplets, whereas the coloured surface illustrates the flame, generated via volume rendering of the temperature field.

Table 1
Overview of the parametric study in terms of equivalence ratio ϕ, overall water loading $Y_W^{ov} = Y_W^g + Y_W^l$, normalized initial droplet diameter a_d/δ_{st}, fuel Lewis number Le_{H_2}, turbulence intensity with respect to stoichiometric laminar burning velocity $u'/S_{L,(\phi=1)}$ and with respect to the laminar burning velocity at the particular equivalence ratio $u'/S_{L,(\phi)}$ and turbulent integral length scale normalized by flame thickness L_{11}/δ_{SDF}.

Case	ϕ	Y_W^{ov}	a_d/δ_{st}	Le_{H_2}	$u'/S_{L,(\phi=1)}$	$u'/S_{L,(\phi)}$	L_{11}/δ_{SDF}
A	0.6	0.0	–	0.2851	4.0	7.3	1.20
B	0.8	0.0	–	0.2851	4.0	5.4	1.82
C	1.0	0.0	–	0.2851	4.0	4.0	2.50
D	0.6	0.1	0.04	0.2851	4.0	7.3	1.20
E	0.8	0.1	0.04	0.2851	4.0	5.4	1.82
F	1.0	0.1	0.04	0.2851	4.0	4.0	2.50
G	0.6	0.1	0.02	0.2851	4.0	7.3	1.20
H	0.8	0.1	0.02	0.2851	4.0	5.4	1.82
I	1.0	0.1	0.02	0.2851	4.0	4.0	2.50
J	0.6	0.0	–	1.0	4.0	11.8	1.01
K	0.8	0.0	–	1.0	4.0	6.3	1.80
L	1.0	0.0	–	1.0	4.0	4.0	2.50
M	0.6	0.1	0.04	1.0	4.0	11.8	1.01
N	0.8	0.1	0.04	1.0	4.0	6.3	1.80
O	1.0	0.1	0.04	1.0	4.0	4.0	2.50
P	0.6	0.1	0.02	1.0	4.0	11.8	1.01
Q	0.8	0.1	0.02	1.0	4.0	6.3	1.80
R	1.0	0.1	0.02	1.0	4.0	4.0	2.50

from detailed chemistry is accurately captured for $0.5 < \phi < 1$, both for the unity and non-unity Lewis number conditions separately. Even though 3*D* DNS with detailed chemistry is possible in the present day, simple chemistry allows for an extensive parametric study as it is performed in the present work. Moreover, it was previously demonstrated that the quantitative differences in terms of flame propagation statistics obtained by the use of a single-step chemistry approach and detailed chemistry are of the same order of magnitude as that of the postprocessing of detailed chemistry DNS data [32,33]. These results further justify the use of a single-step chemistry approach in the current analysis. The turbulence is considered through the imposition of the turbulent flow field with root mean square of velocity fluctuations over laminar stoichiometric flame speed $u'/S_{L,(\phi=1)} = 4.0$, and integral length scale over unstretched stoichiometric thermal flame thickness $L_{11}/\delta_{st} = 2.5$. The parameters were chosen to reflect combustion in the practically relevant thin reaction zones regime [34]. The choice of $u'/S_{L,(\phi=1)} = 4$ is made to ensure that turbulence does not entirely disrupt the flame structure, but still wrinkles the flame and perturbs the preheat zone. Simultaneously, selecting $L_{11}/\delta_{st} = 2.5$ aims to ensure the natural development of turbulence structures within the computational domain with respect to the use of periodic boundary conditions. At the same time, it guarantees a sufficient number of independent samples for averaging in the homogeneous directions. Together with the resolution of the Kolmogorov scale and the flame structure, these parameters enable DNS of all turbulent scales with adequate resolution and follow the usual best practice guidelines. The turbulence is initialized by superimposing it onto the laminar initial conditions and is sustained through a turbulent inflow that has the same spectrum and parameters of the initial turbulent flow field. At the time $t = 4.2 \, t_{chem}$ quantities are slowly varying with time and small fluctuations do not affect the qualitative statements made in this work. As the introduction states, differential diffusion of the fuel is expected to play an important role in hydrogen/air combustion. In the context of this work, the Lewis number of hydrogen is assumed to be 0.2851 and for all other species (oxygen and water vapour) it is assumed to be unity. While this study employs certain simplifying assumptions, particularly in the modelling of droplets (e.g. uniform initial diameter mist, constant liquid phase density), it is important to stress that the objective of this investigation is not to replicate a practical technological application, but rather to achieve a more profound comprehension of the fundamental physics governing the interaction between liquid water and non-unity Lewis number flames. Moreover, the methodology employed has been extensively acknowledged in the academic literature [6,35–39], serving as

supplementary evidence for the validity of the present results. For the subsequent discussion, the thickness of flame δ_{SDF} (here based on the surface density function, $SDF = |\nabla c|$), and the density ratio γ will play key roles, which are defined as:

$$\delta_{SDF} = \frac{1}{max\langle|\nabla c|\rangle} \tag{6}$$

$$\gamma = \frac{\rho_u}{\rho_b} \tag{7}$$

The symbol $\langle Q \rangle$ stands for the average conditional on the progress variable c, which in this study is computed from the oxygen concentration:

$$c = \frac{Y_O^0 - Y_O}{Y_O^0 - Y_O^b} \tag{8}$$

where the superscripts 0 and b refer to unburned conditions and chemical equilibrium, respectively.

3. Results and discussion

In the results section, we will first present the effects of water injection and the initial diameter of the water droplets on the characteristics of hydrogen/air flame propagation. Next, the effect of preferential diffusion will be isolated to understand how the flame-water interaction is affected by this phenomenon.

3.1. Effects of initial diameter of water droplets

The DNS database is presented in Table 1, with the different parameters considered in this work. In this subsection, first the simulations with hydrogen Lewis number $Le_{H_2} = 0.2851$ are considered (i.e. cases A-I). The main effect of liquid water injection is the cooling due to the evaporation of the droplets. The evaporation of liquid water droplets mainly affects the temperature field, leaving the reaction progress variable field relatively unaffected. It can be observed from Fig. 2 that the iso-surfaces of the reaction progress variable and non-dimensional temperature are considerably different. The surface related to the reaction progress variable, the one on the left, presents wrinkling only due to turbulence, while the iso-surface on the right, related to non-dimensional temperature, shows small dimples where the droplets evaporate and deform the iso-surface by extracting the latent heat of evaporation. In the cases considered here, the differences between
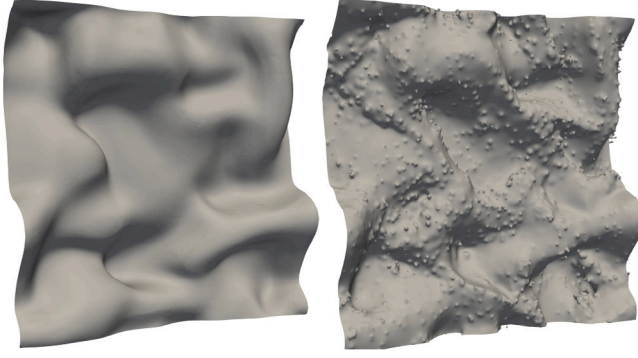
Fig. 2. Reaction progress variable (left) and non-dimensional temperature (right) iso-surfaces with value 0.9 for both these quantities. The results are taken at $t = 1.0$ t_{chem}.

temperature and progress variable are related to the heat extraction due to water evaporation and the Lewis number, of hydrogen, which is different from unity. A significant effect associated with Lewis numbers smaller than unity is the presence of local super-adiabatic spots within the burned gas where the flame surface is convex towards the reactants. This is a consequence of the faster focusing of fuel into the reaction zone than the defocusing of heat out of the reaction zone. Just the opposite combination gives rise to relatively low temperatures in the regions of a given c iso-surface where it is concave towards the reactants. This behaviour is observed in all simulated cases considered in this subsection because hydrogen is always diffusing faster than temperature, air and water vapour.

Fig. 3 shows the distributions of non-dimensional temperature $T = (\hat{T} - \hat{T}_0)/(\hat{T}_{ad,(\phi)} - \hat{T}_0)$ and gaseous water concentration Y_W^g arising from evaporation of injected water droplets in the $x-y$ mid-plane of the simulations with injection of water droplets with initial $a_d/\delta_{st} = 0.04$ (i.e. large droplets within the parameter range considered here). In these cases, the presence of the super-adiabatic temperature spots in the burned gas are still observable because the evaporation effect is not strong enough to decrease the temperature sufficiently. From the right column of Fig. 3, it becomes clear that the evaporation effects are substantial only in the stoichiometric and mildly lean cases. This is because the mean burned gas temperature decreases with the equivalence ratio, even though local super-adiabatic temperature zones exist, as observable in Fig. 4 which shows the probability density function of the non-dimensional temperature inside the reaction zone and burned gas region of the flame. The weakening of thermal expansion effects (reflected in a decrease in γ shown in Table 2) for a decrease in equivalence ratio acts to reduce the mean velocity within the flame which also increases the residence time of the droplets ahead of the reaction zone and burned gas region. As the droplets quickly accelerate to the velocity of the carrier phase, the average droplet velocity decreases with the decrease of the equivalence ratio, as noted earlier by Hasslberger et al. [40] for n-heptane flames. The well-known a_d^2 law [41] indicates that the evaporation rate follows a non-linear trend with respect to the initial droplet diameter. For this reason, the expected effects from the water evaporation in the cases with $a_d/\delta_{st} = 0.02$ are substantially stronger than for the cases with initial $a_d/\delta_{st} = 0.04$. Fig. 5 shows the distributions of temperature, and the water concentration arising from the evaporation of injected water droplets in the $x-y$ mid-plane for the cases with initial $a_d/\delta_{st} = 0.02$ (i.e. small droplets within the parameter range considered here). It can be seen from Fig. 5 that in the burned gas side, the gaseous water concentration arising from the evaporation of water droplets (i.e. excluding water produced by chemical reaction) reaches close to the imposed overall value of water in the stoichiometric and mildly lean cases in contrast to the corresponding cases with initial $a_d/\delta_{st} = 0.04$. This behaviour arises because of the enhancement of

Table 2
Density jump γ at different equivalence ratio ϕ.

ϕ	γ
0.6	6.7
0.8	7.6
1.0	7.9

the evaporation rate with a decrease in the initial droplet diameter. The rapid rate of evaporation induces a cooling effect as a result of the extraction of latent heat and dilution of fuel concentration, which is reflected in the reduced likelihood of the occurrence of the super-adiabatic temperature pockets in the burned gas in the cases with initial $a_d/\delta_{st} = 0.02$ in comparison to the corresponding cases with initial $a_d/\delta_{st} = 0.04$. The average burned gas temperature has been found to be mostly smaller than that in the cases with larger water droplets. Both the extent of flame wrinkling and flame topology change as a result of evaporation of water droplets. For example, a comparison between Figs. 3 and 5 reveals that finger-like flame wrinkles seen for initial $a_d/\delta_{st} = 0.04$ cases are much less apparent in the cases with initial $a_d/\delta_{st} = 0.02$.

Fig. 6 shows the quantitative differences between the cases by means of the temporal evolution of the gaseous water vapour concentration arising from droplet evaporation averaged within the flame. The trend is monotonic with respect to the equivalence ratio, i.e. the stoichiometric case has the highest concentration followed by the mildly lean and strongly lean cases, as higher flame temperature acts to increase the level of evaporation of the injected droplets. Moreover, a substantial increase in gaseous water concentration with the decrease in droplet diameter can be observed from Fig. 6. In the cases with the smaller droplets, the gaseous water concentration reaches the overall water concentration Y_W^{ov} considered for the $\phi = 1.0$ case, as demonstrated already in Fig. 5. In the cases with the larger droplets, the water vapour concentration remains always below 20% of the imposed overall water concentration. The decrease observed in gaseous water concentration within the flame for the case with $\phi = 1$ and $a_d/\delta_{st} = 0.02$ is attributed to the displacement of the flame brush position induced by turbulence. This phenomenon arises due to the significantly longer evaporation timescale compared to the turbulent and chemical timescales. However, this effect is not evident for other equivalence ratios, as the flame moves towards the outlet where higher water concentration is present, as depicted in Fig. 5. An essential characteristic of the flame is its thickness, which is strongly affected by the temperature of the burned gas. An increase in flame thickness makes the flame less susceptible to wrinkling as discussed in literature [42–44].

Fig. 7 shows the temporal evolution of the flame thickness compared to the cases without water injection. In all the simulations, the flame thickens with water injection, and this intensifies with an increase in evaporation intensity for small droplets. The temporal evolution of δ_{SDF}/δ_{st} suggests that the gaseous water concentration continues to grow for both lean cases since the flame thickness continues to grow also at later times of the simulation. At the same time, the steam concentration reaches a plateau in the stoichiometric case with small water droplets. In addition to the flame thickness the water injection affects the overall burning rate, which is quantified by the turbulent burning velocity $S_T = \int \dot{\omega}_c dV/\rho_u A_0$ where $\dot{\omega}_c$ is the reaction rate of reaction progress variable, ρ_u is the unburned gas density and A_0 is the projected flame area in the direction of mean flame propagation. The burning velocity is determined by two factors, namely, the flame surface area and Ω, which is the reactant consumption rate per unit flame area under turbulent conditions normalized by the corresponding value under laminar conditions. The quantity Ω is defined as:

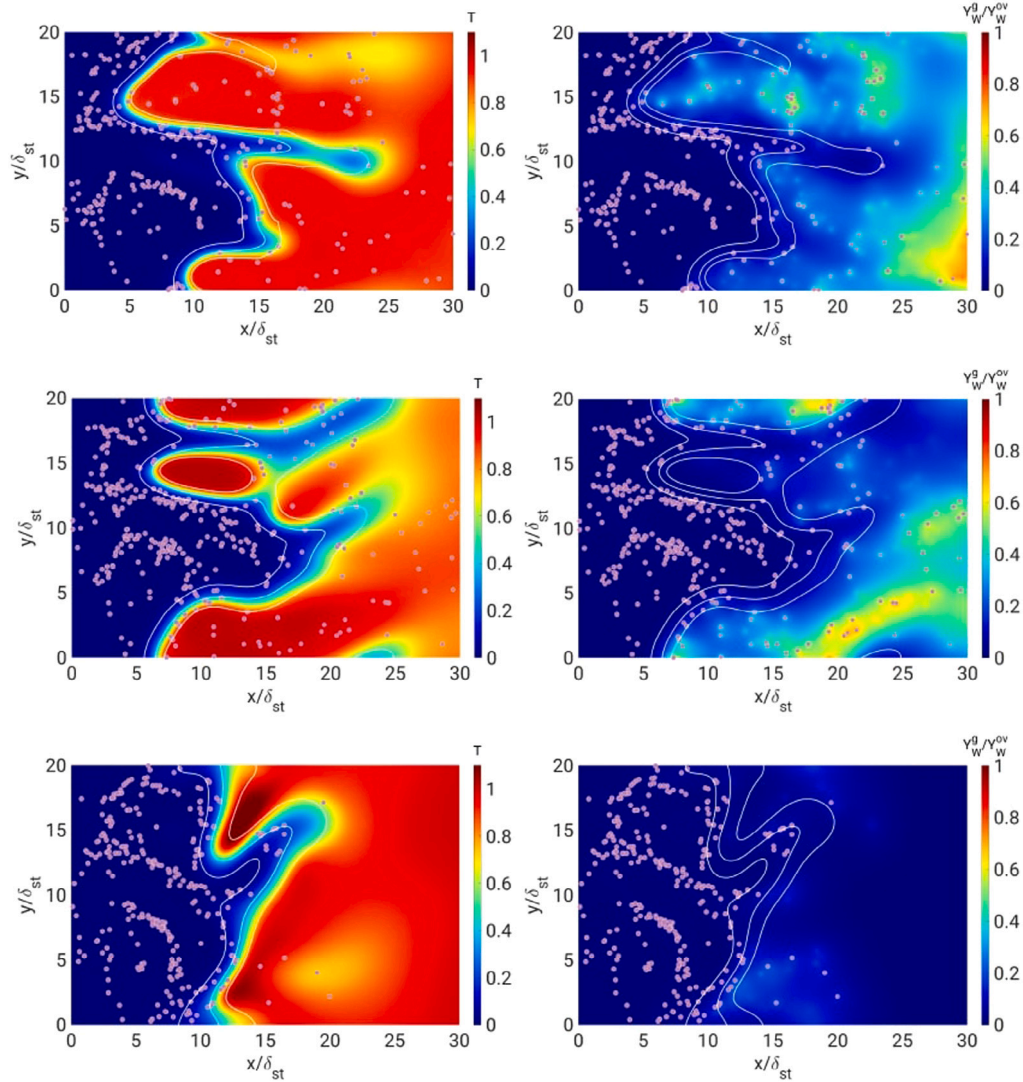$$\Omega = \frac{S_T}{S_{L,(\phi)}} \frac{A_0}{A_c} \tag{9}$$

Fig. 3. The distributions of non-dimensional temperature (left), and gaseous water concentration arising from the evaporation of injected water droplets (right) in the $x - y$ mid-plane at $t = 4.2\ t_{chem}$. From top to bottom, the equivalence ratio is $\phi = 1.0$, 0.8 and 0.6. The initial droplet size is $a_d/\delta_{st} = 0.04$ in all cases. The pink dots represent the water droplets (not to the scale). The white curves represent contours of $c = 0.1, 0.5, 0.9$ (left to right).
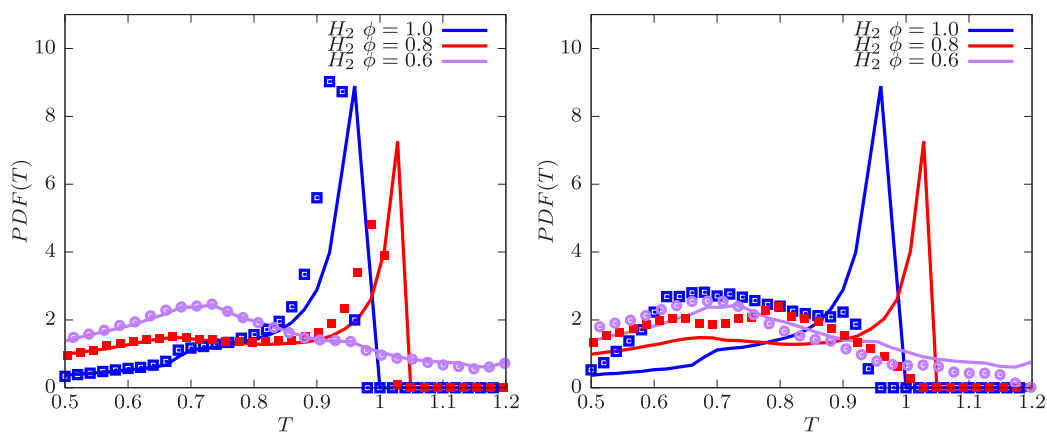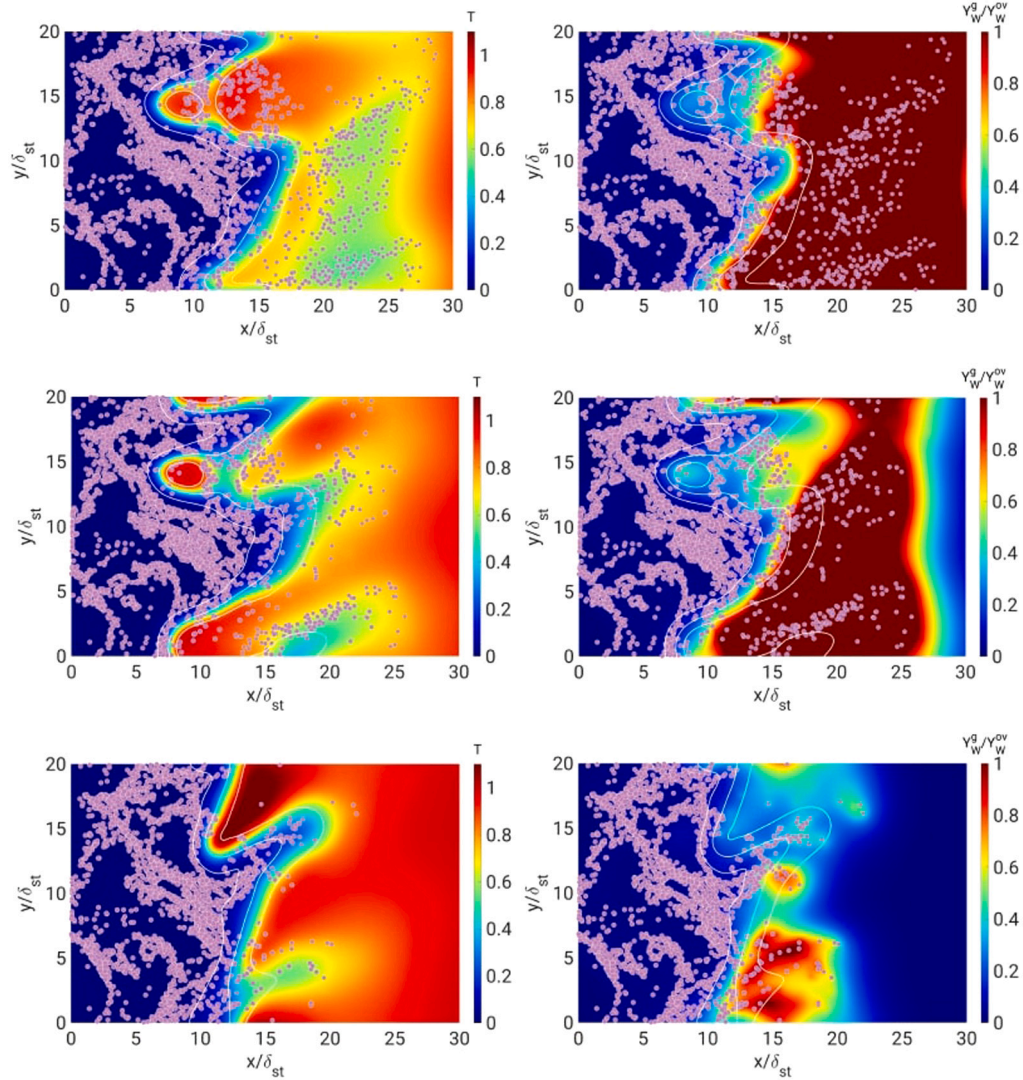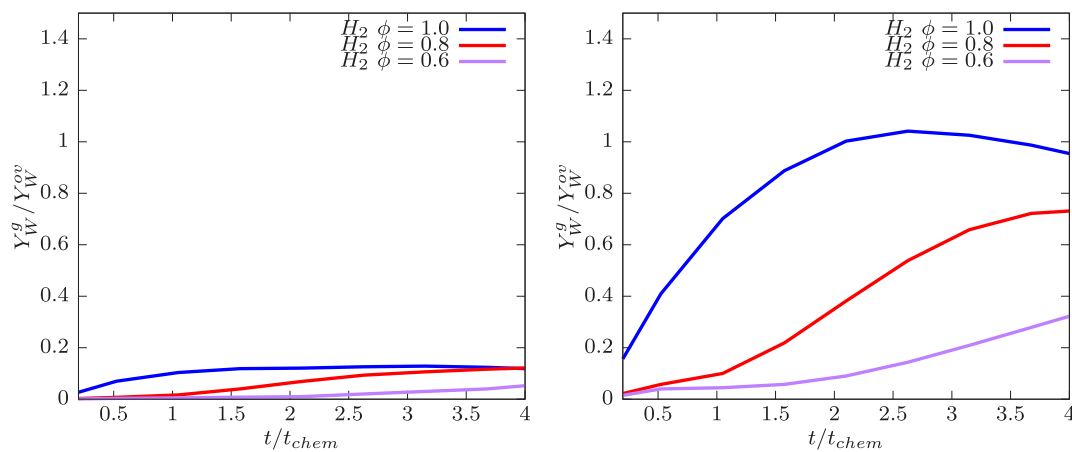

Fig. 4. Probability density function of the non-dimensional temperature inside the hot region of the flame ($0.7 \leq c \leq 0.99$) with initial $a_d/\delta_{st} = 0.04$ (left) and with initial $a_d/\delta_{st} = 0.02$ (right) at $t = 4.2\ t_{chem}$. The continuous lines are related to the cases without water injection, and the symbols are related to those with water droplets injection.

Fig. 5. The distributions of non-dimensional temperature (left), and gaseous water concentration arising from the evaporation of injected water droplets (right) in the $x - y$ mid-plane at $t = 4.2\ t_{chem}$. From top to bottom, the equivalence ratio is $\phi = 1.0,\ 0.8$ and 0.6. The initial droplet size is $a_d/\delta_{st} = 0.02$ in all cases. The pink dots represent the water droplets (not to the scale). The white curves represent contours of $c = 0.1, 0.5, 0.9$ (left to right).

Fig. 6. Time evolution of gaseous water concentration inside the flame ($0.1 \leq c \leq 0.9$) with $a_d/\delta_{st} = 0.04$ (left) and with $a_d/\delta_{st} = 0.02$ (right).

Fig. 7. Time evolution of the normalized flame thickness δ_{SDF}/δ_{st} with initial $a_d/\delta_{st} = 0.04$ (left) and with initial $a_d/\delta_{st} = 0.02$ (right). The continuous lines are related to the cases without water injection, and the symbols are related to those with water droplets injection.
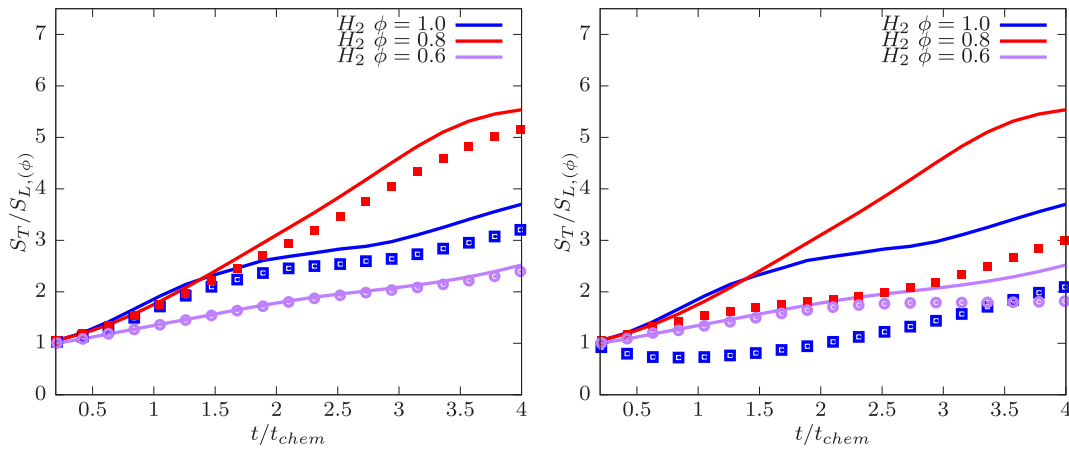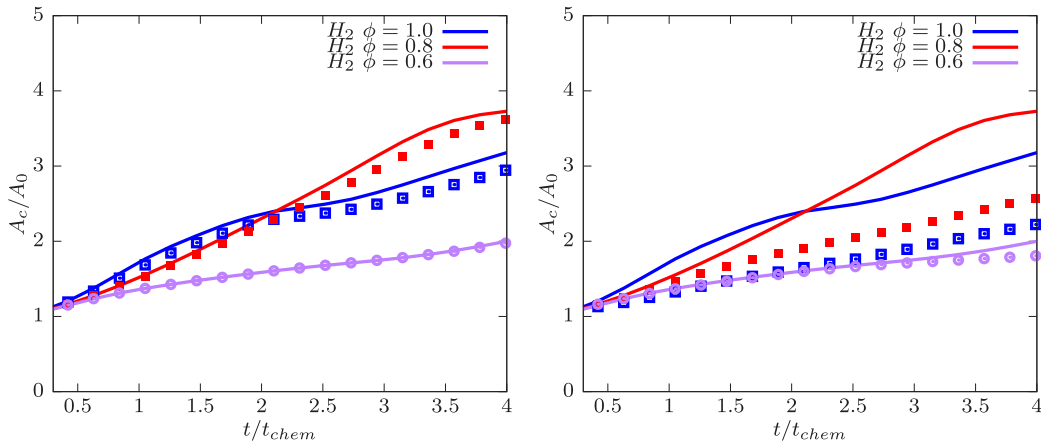

Fig. 8. Time evolution of the normalized turbulent burning velocity $S_T/S_{L,(\phi)}$ with initial $a_d/\delta_{st} = 0.04$ (left) and with initial $a_d/\delta_{st} = 0.02$ (right). The continuous lines are related to the cases without water injection, and the symbols are related to those with water droplets injection.

Fig. 9. Time evolution of the normalized flame area A_c/A_0 with initial $a_d/\delta_{st} = 0.04$ (left) and with initial $a_d/\delta_{st} = 0.02$ (right). The continuous lines are related to the cases without water injection, and the symbols are related to those with water droplets injection.

The symbol A_c stands for the flame area evaluated based on the SDF:

$$A_c = \int |\nabla c| dV \tag{10}$$

Moreover, the normalized flame surface area A_c/A_0 provides the measure of flame wrinkling. A value of $\Omega = 1.0$ indicates that the increase of the burning rate due to chemical reaction occurs solely due to the augmentation of the flame surface area, which is often referred to as Damköhler's first hypothesis [45,46]. However, $\Omega > 1$ is obtained for flames with characteristic Lewis numbers smaller than unity. The effects of water droplet injection on the evolution of $S_T/S_{L,(\phi)}$ are shown in Fig. 8. The general effect is a decrease in the growth of $S_T/S_{L,(\phi)}$ with the injection of liquid water droplets. When
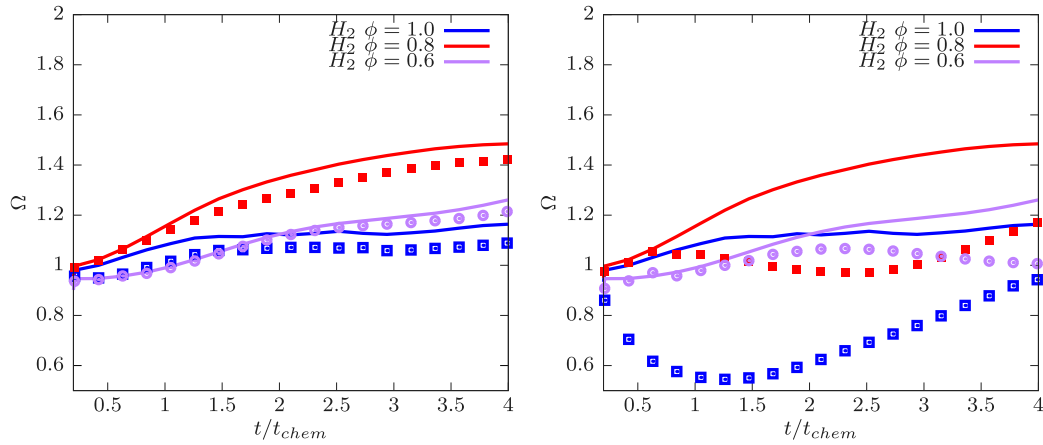
Fig. 10. Time evolution of burning rate per unit area Ω with initial $a_d/\delta_{st} = 0.04$ (left) and with initial $a_d/\delta_{st} = 0.02$ (right). The continuous lines are related to the cases without water injection, and the symbols are related to those with water droplets injection.
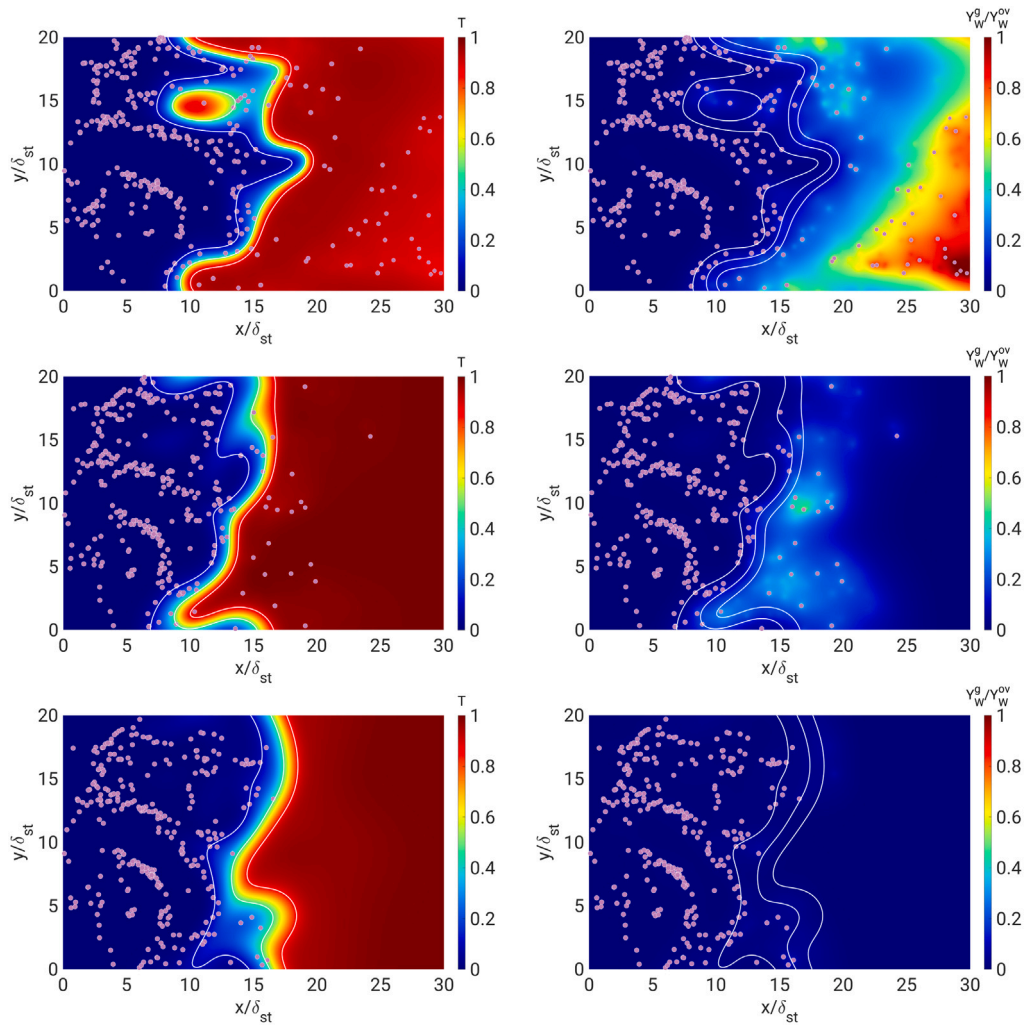

Fig. 11. The distributions of non-dimensional temperature (left), and gaseous water concentration arising from the evaporation of injected water droplets (right) in the $x - y$ mid-plane at $t = 4.2\, t_{chem}$. From top to bottom, the equivalence ratio is $\phi = 1.0, 0.8$ and 0.6. The initial droplet size is $a_d/\delta_{st} = 0.04$ in all cases. The pink dots represent the water droplets (not to the scale). The white curves represent contours of $c = 0.1, 0.5, 0.9$ (left to right).

the evaporation intensifies, the growth of $S_T/S_{L,(\phi)}$ is strongly affected and a non-monotonic temporal evolution is observed for some cases. To understand the temporal evolution of $S_T/S_{L,(\phi)}$ in response to water droplet injection, the temporal evolutions of A_c/A_0 and Ω are shown in Figs. 9 and 10, respectively for both water droplet sizes and the cases

without water injection. It can be seen from Fig. 9 that the flame surface area is not strongly affected for the larger water droplets, because the evaporation rate is not high enough. The flame surface area for the cases with small water droplet injection is considerably lower than that without water injection. However, the difference is substantial only for
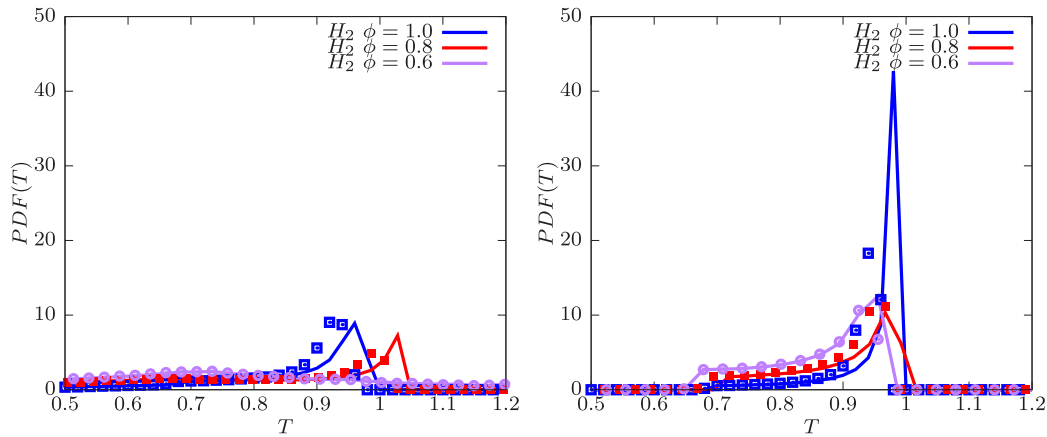
Fig. 12. Probability density function of the non-dimensional temperature inside the hot region of the flame ($0.7 \le c \le 0.99$) with $Le_{H_2} \neq 1$ (left) and with $Le_{H_2} = 1$ (right) at $t = 4.2$ t_{chem}. The continuous lines are related to the cases without water injection, and the symbols are related to those with initial droplet diameter $a_d/\delta_{st} = 0.04$.

Fig. 13. Time evolution of normalized turbulent burning velocity $S_T/S_{L,(\phi)}$ with $Le_{H_2} \neq 1$ (left) and with $Le_{H_2} = 1$ (right). The continuous lines are related to the cases without water injection, and the symbols are related to those with initial droplet diameter $a_d/\delta_{st} = 0.04$.
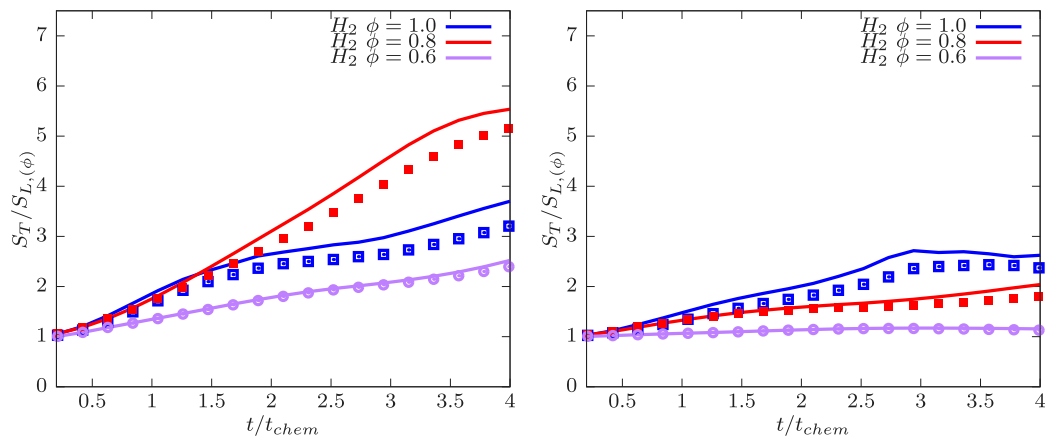

Fig. 14. Time evolution of the normalized flame area A_c/A_0 with $Le_{H_2} \neq 1$ (left), and with $Le_{H_2} = 1$ (right). The continuous lines are related to the cases without water injection, and the symbols are related to those with initial droplet diameter $a_d/\delta_{st} = 0.04$.
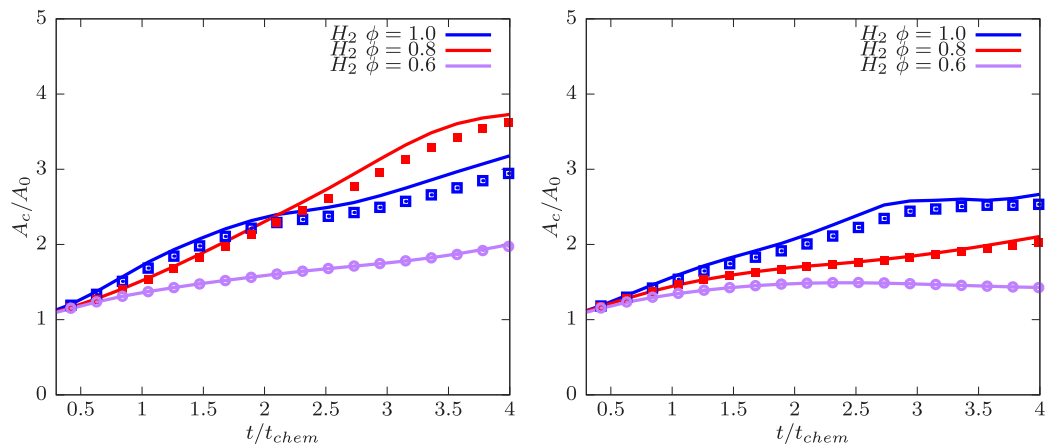
the stoichiometric and the mildly lean cases, while for the strongly lean case, it can only be discerned at later times. Note that the reaction progress variable, i.e. the quantity through which the surface area is calculated, is not directly affected by the water evaporation. Similar results were obtained by Hasslberger et al. [40] for n-heptane/air flames with water injection. A comparison of Figs. 8 and 9 reveals that

the temporal evolution of A_c/A_0 is not sufficient to explain the non-monotonic trend of $S_T/S_{L,(\phi)}$ evolution, as observed in Fig. 8. It can be seen from Fig. 10 that Ω is not strongly affected by injection of large water droplets but some deviations of the trends, between the cases with water and without, are visible for all equivalence ratios. However, Ω values for small water droplet cases are significantly different from
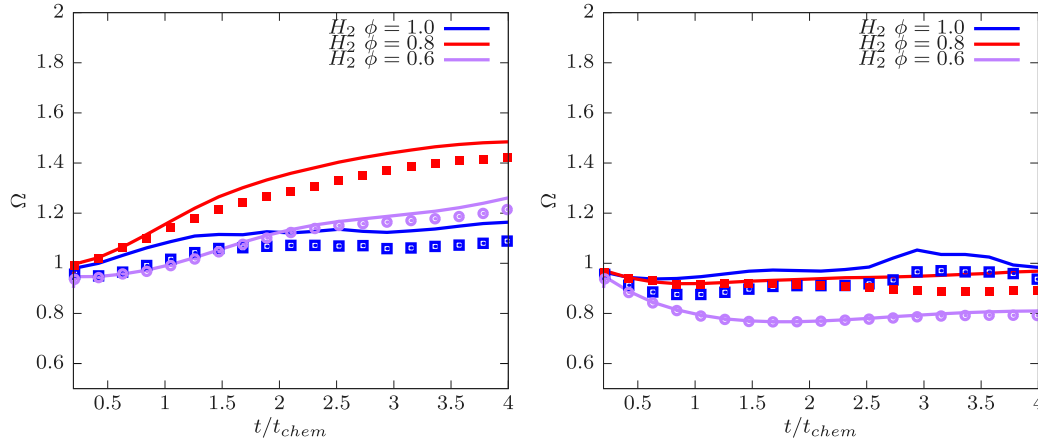
Fig. 15. Time evolution of burning rate per unit area Ω with $Le_{H_2} \neq 1$ (left), and $Le_{H_2} = 1$ (right). The continuous lines are related to the cases without water injection, and the symbols are related to those with initial droplet diameter $a_d/\delta_{st} = 0.04$.

the purely gaseous cases without water injection. In the stoichiometric case with small water droplets, Ω assumes a value much smaller than unity, thus demonstrating that this mechanism is responsible for the decay of $S_T/S_{L,(\phi)}$ with time under this condition. The above results indicate that the cooling effects induced by the evaporation of water droplets, as a result of latent heat extraction (major effect) and dilution of fuel concentration (minor effect) within the flame, act to thicken the flame and reduce the burned gas temperature. The combination of reduced burned gas temperature and thicker flame acts to reduce the extent of flame wrinkling and makes the flame more prone to partial quenching. It is also interesting to note the presence of non-monotonic behaviour of Ω and A_c/A_0 with the equivalence ratio. This is a result of the competition between the ratio of root-mean-square (rms) value of turbulent velocity to actual laminar flame speed $u'/S_{L,(\phi)}$, normalized wrinkling length scale L_{11}/δ_{SDF} and effects of preferential diffusion, which will be discussed in more detail in the next subsection.

3.2. Preferential diffusion effects

The important effects of preferential diffusion are isolated by comparing the results of non-unity Le_{H_2} simulations with the corresponding simulations with $Le_{H_2} = 1.0$. Table 1 shows the parameters for the simulations with unity Lewis number (cases J-R) without droplets and for both droplet sizes. The strength of preferential diffusion effects can be expressed with the help of an effective Lewis number Le_{eff} which describes the overall mass diffusion behaviour of the mixture and can be calculated through the Bechtold–Matalon formula, which is an equivalence ratio weighted average of the fuel and oxidizer Lewis number, which for lean mixtures reads [47]:

$$Le_{eff} = 1 + \frac{(Le_{O_2} - 1) + (Le_{H_2} - 1)A}{1 + A};$$
$$A = 1 + \beta(\frac{1}{\phi} - 1). \tag{11}$$

Eq. (11) depends on the Zeldovich number β, that in our case is 5.0 [48]. The effective Lewis numbers for cases A-I are given in Table 3 as a function of the equivalence ratio, while for cases J-R the effective Lewis number is identical to unity.

A qualitative assessment of the distinct behaviour of the flame when preferential diffusion is disabled is evident in Fig. 11 for the large water droplets (i.e. cases M-O), illustrating the non-dimensional temperature fields (left) and gaseous water concentration (right). In all three cases, there are no super-adiabatic regions, indicating that the maximum normalized temperature remains unity. Additionally, the temperature fields exhibit reduced levels of stratification and higher homogeneity compared to cases with preferential diffusion. Furthermore, these flames reveal reduced wrinkling of the flame surface and a lower

Table 3
Effective Lewis number Le_{eff} at different equivalence ratio ϕ, for the present thermo-chemistry.

ϕ	Le_{eff}
0.6	0.42
0.8	0.51
1.0	0.64

evaporation rate, particularly evident in lean cases compared to the corresponding simulations with $Le_{H_2} \neq 1$. A quantitative validation of the absence of super-adiabatic regions, especially under lean conditions when the Lewis number is 1.0, is provided in Fig. 12, where non-dimensional temperature PDFs are presented for cases with non-unity Lewis numbers on the left and unity Lewis numbers on the right. From the PDFs in Fig. 12, it is evident that the peak of probability in the distribution is higher in the cases with $Le_{H_2} = 1$ than the cases with preferential diffusion, suggesting a lower temperature stratification. Moreover, those peaks are always at a position of $T \leq 1$. Furthermore, the absence of a tail in the region $T > 1$ confirms the absence of super-adiabatic regions when preferential diffusion is absent. However, the effect of evaporation of liquid water droplets is qualitatively similar for non-unity and unity Lewis number conditions. The peaks of the non-dimensional temperature PDF move towards cooler regions and the distributions become broader in the cases with water injection due to the thermal stratification caused by the local cooling obtained by the evaporation of the droplets. This can be deduced from the decrease of the magnitude of PDFs, which suggests an increase of its width because the PDF integrates to unity to satisfy the normalization constraint. The presence of preferential diffusion also influences the evolution of the turbulent burning velocity. Fig. 13 shows the evolution of the turbulent burning velocity for the cases with non-unity Lewis number on the left and for the unity Lewis number on the right. The temporal increase of the turbulent burning velocity when the preferential fuel diffusion is switched off has a smaller slope than in the cases with $Le_{H_2} \neq 1$, which clearly underlines the preferential diffusion effects for cases A-I, which are characterized by $Le_{eff} < 1$. Furthermore, without preferential diffusion, $S_T/S_{L,(\phi)}$ monotonically increases with ϕ. The stoichiometric case reaches the highest value, followed by the slightly lean and strongly lean cases, respectively for the unity Lewis number condition. The strongly lean case, in particular, has an almost constant value of $S_T/S_{L,(\phi)}$ for $Le_{H_2} = 1$. Referring to Table 1 it becomes clear that the flame wrinkling is dominated by the small ratio of normalized integral length scale L_{11}/δ_{SDF} (which is smallest and of the order of unity for the cases with $\phi = 0.6$) rather than the ratio of rms turbulent velocity to actual laminar flame speed $u'/S_{L,(\phi)}$ (which is highest for
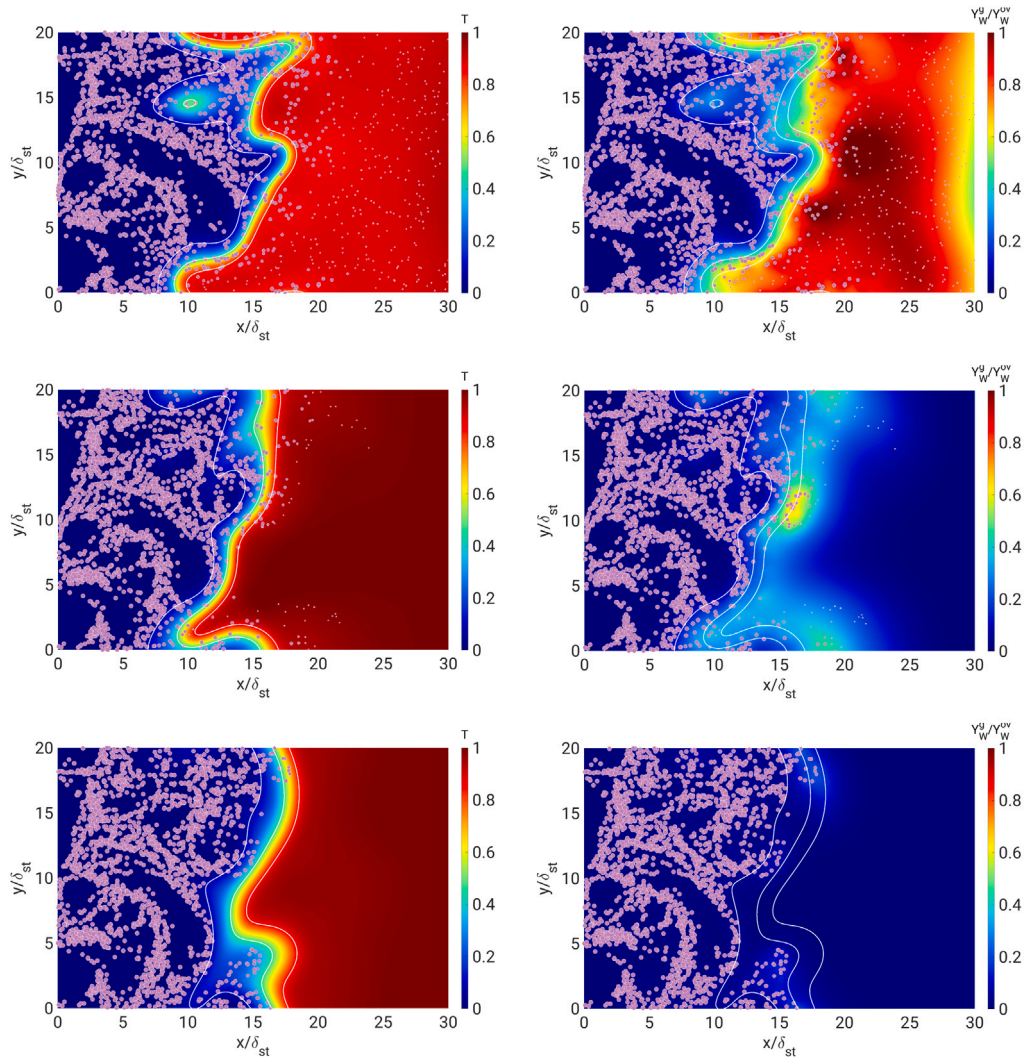
Fig. 16. The distributions of non-dimensional temperature (left), and gaseous water concentration arising from the evaporation of injected water droplets (right) in the $x - y$ mid-plane at $t = 4.2\, t_{chem}$. From top to bottom, the equivalence ratio is $\phi = 1.0$, 0.8 and 0.6. The initial droplet size is $a_d/\delta_{st} = 0.02$ in all cases. The pink dots represent the water droplets (not to the scale). The white curves represent contours of $c = 0.1, 0.5, 0.9$ (left to right).

the cases with $\phi = 0.6$). For the cases with $Le_{H_2} \neq 1$, Le_{eff} grows with ϕ and the effects of preferential diffusion thus become less intense. However, preferential diffusion needs a wrinkled flame in order to become effective. As can be seen from Fig. 14, the $\phi = 0.6$ flames are characterized by a small amount of wrinkling. Hence, despite the small effective Lewis number for cases A,D,G, preferential diffusion effects are not pronounced. By contrast, the flame is much more effectively wrinkled for cases B,E,H with $\phi = 0.8$ which enhances preferential diffusion effects and ultimately leads to larger values of $S_T/S_{L,(\phi)}$ and A_c/A_0 for the $\phi = 0.8$ compared to the $\phi = 1.0$ case in contrast to cases J-O with $Le_{H_2} = 1$, where the effective Lewis number is unity. In other words, the evolution of A_c is mainly determined by turbulence-induced wrinkling, while preferential diffusion acts only to amplify this phenomenon. Finally, the analysis performed earlier on Ω and A_c is now repeated for the cases with $Le_{H_2} = 1$ and compared with that for the cases with $Le_{H_2} \neq 1$, to better understand the different trends observed in Fig. 13. From Damköhler's first hypothesis and the results of previous studies [45,46,49], we expect that in the absence of preferential diffusion (i.e. $Le_{H_2} = 1$) the value of Ω should be around unity. Fig. 15 confirms the previous hypothesis, at least approximately for the cases with $\phi = 1.0$ and 0.8. In both cases, the value of Ω fluctuates around unity over the course of the simulations. In the cases J,O with $\phi = 0.6$, Ω stabilizes at 0.8 instead of 1.0. This behaviour arises

because the leanest case is prone to partial quenching of the flame due to stretch effects when $Le_{H_2} = 1$ at this equivalence ratio.

The effects of water evaporation when $Le_{H_2} = 1$ are slightly weaker compared to the corresponding cases with $Le_{H_2} \neq 1$, in particular for the most fuel lean case considered here. This can again be explained by the preferential diffusion effects potentially leading to the presence of super-adiabatic temperature regions. These regions amplify the heat flux from the gaseous phase to the liquid phase, thereby enhancing the evaporation rate. However, they also induce an increase in the droplet's velocity due to enhanced thermal expansion, subsequently diminishing the potential residence time within the burned gas region. These two opposing influences result in a faster evaporation of the droplets in comparison to that in the corresponding $Le_{H_2} = 1.0$ cases with the same ϕ. The more pronounced impact of increased heat flux overshadows the effects on droplet residence time, especially given its inherently shorter duration compared to the average lifetime of droplets in the scenarios under consideration. As a result, the impact of liquid water injection is weaker in the unity Lewis number cases than in the non-unity Lewis number cases. For completeness, the analysis regarding the effects of preferential diffusion is repeated for the small water droplets (cases P-R). Fig. 16 shows the non-dimensional temperature and concentration of gaseous water resulting only from evaporation, presented on the left and right sides respectively, for cases characterized by unity Lewis
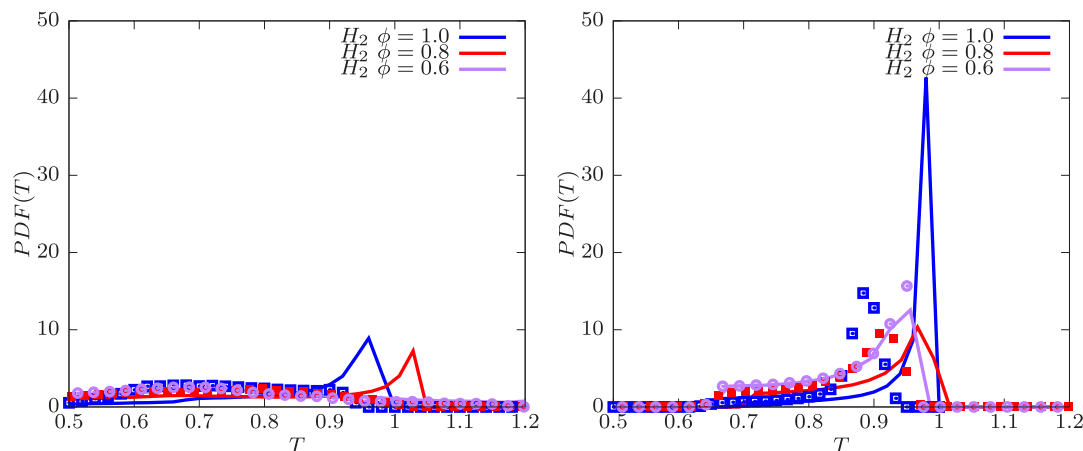
Fig. 17. Probability density function of the non-dimensional temperature inside the hot region of the flame ($0.7 \leq c \leq 0.99$) with $Le_{H_2} \neq 1$ (left) and with $Le_{H_2} = 1$ (right) at $t = 4.2$ t_{chem}. The continuous lines are related to the cases without water injection, and the symbols are related to those with initial droplet diameter $a_d/\delta_{st} = 0.02$.

number and initial water droplet diameters of $a_d/\delta_{st} = 0.02$. Fig. 16 confirms that the absence of super-adiabatic regions in cases without preferential diffusion substantially impacts evaporation, surpassing the influence of other factors such as flow acceleration. The general behaviour observed in Fig. 16 is very similar to Fig. 11 with higher amounts of water vapour observed for the smaller droplets. The effects of evaporation can be further assessed through PDFs of temperature, as shown in Fig. 17. By comparing the right part of Fig. 17 with Fig. 12 for small and large droplets respectively, it can be seen that the effects of preferential diffusion are qualitatively similar in both cases, but somewhat more pronounced for the small droplets due to stronger evaporation.

4. Conclusions

The effects of liquid water injection on the combustion characteristics of statistically planar hydrogen/air premixed turbulent flames have been analysed in the present work based on a series of carrier-phase DNS. The following conclusions can be drawn:

- The non-unity Lewis number effects are most prominent in the mildly fuel-lean case (i.e. $\phi = 0.8$) and are less significant for the strongly lean cases (i.e. $\phi = 0.6$) because thicker flames in these cases act to reduce the extent of wrinkling compared to the mildly fuel-lean cases.
- The evaporation characteristics are highly dependent on the initial size of the water droplets, which has consequences for the technical application of water injection.
- Water injection tends to attenuate the effects of differential diffusion arising from non-unity Lewis number. This attenuation is particularly strong for small water droplets due to their high evaporation rate.
- The water injection effects on the flame surface area have been found to be negligible for the strongly fuel-lean cases but are more intense in the mildly fuel-lean and stoichiometric cases.
- The reactant consumption rate per unit flame area decreases with increasing water evaporation intensity due to the cooling effect.
- The evolution of burning rate per unit area and flame area are strongly affected by the water injection in the absence of preferential diffusion.
- Further, the absence of preferential diffusion indirectly affects the interaction between the flame and the liquid phase. This is a consequence of the maximum burned gas temperature reached in the system which in turn affects the evaporation rate within the flame.

The above findings indicate that increased wrinkling results in stronger preferential diffusion effects and an increased turbulent burning velocity. Consequently, the cooling mechanism within the system (e.g. water droplet evaporation) inhibits or counteracts certain characteristic phenomena of hydrogen combustion, such as the growth of burning rate per unit area and enhancement of flame surface area. Conversely, deactivating preferential diffusion in a numerical experiment yields a less wrinkled flame with a decreased burning rate per unit area. Moreover, the liquid water evaporation decreases due to the lower maximum temperature attained by the system for the unity Lewis number simulations.

While the qualitative analysis reported in this work offers valuable insights into the general behaviour and is underlined by sound physical arguments, quantitative results may be influenced to some extent by the simplifying assumptions adopted. Consequently, further analysis with a more detailed description of chemistry and transport will be desirable to confirm the present findings and additionally to analyse the effect of water injection on NO_x emissions which are known to be temperature sensitive.

CRediT authorship contribution statement

Riccardo Concetti: Writing – original draft, Visualization, Software, Methodology, Formal analysis. **Josef Hasslberger:** Writing – review & editing, Supervision, Software, Methodology, Conceptualization. **Nilanjan Chakraborty:** Writing – review & editing, Software, Methodology, Conceptualization. **Markus Klein:** Writing – review & editing, Supervision, Resources, Methodology, Conceptualization.

Declaration of competing interest

The authors declare that they have no known competing financial interests or personal relationships that could have appeared to influence the work reported in this paper.

Data availability

Data will be made available on request.

References

[1] Cârdu M, Baica M. Gas turbine installation with total water injection in the combustion chamber. Energy Convers Manage 2002;43(17):2395–404.

[2] Tauzia X, Maiboom A, Shah SR. Experimental study of inlet manifold water injection on combustion and emissions of an automotive direct injection diesel engine. Energy 2010;35(9):3628–39.

[3] Omidvar A, Mahdavi A, Mehryar R. A simulated study on the effect of water temperature on cooling efficiency of water mist fire extinguishers. J Therm Eng 2020;6(4):460–73.

[4] Koroll G, Mulpuru S. The effect of dilution with steam on the burning velocity and structure of premixed hydrogen flames. Proc Combust Inst 1988;21(1):1811–9.

[5] Koroll G, Kumar R, Bowles E. Burning velocities of hydrogen-air mixtures. Combust Flame 1993;94(3):330–40.

[6] Hasslberger J, Ozel-Erol G, Chakraborty N, Klein M, Cant S. Physical effects of water droplets interacting with turbulent premixed flames: A Direct Numerical Simulation analysis. Combust Flame 2021;229(32):111404.

[7] Sivashinsky G. Diffusional-thermal theory of cellular flames. Combust Sci Technol 1977;15(3–4):137–45.

[8] Sivashinsky GI. Instabilities, pattern formation, and turbulence in flames. Annu Rev Fluid Mech 1983;15(1):179–99.

[9] Libby PA, Liñń A, Williams FA. Strained premixed laminar flames with nonunity Lewis numbers. Combust Sci Technol 1983;34(1–6):257–93.

[10] Clavin P, Joulin G. Premixed flames in large scale and high intensity turbulent flow. J Physique Lett 1983;44(1):1–12.

[11] Abdel-Gayed R, Bradley D, Hamid M, Lawes M. Lewis number effects on turbulent burning velocity. Proc Combust Inst 1985;20(1):505–12.

[12] Law CK, Kwon O. Effects of hydrocarbon substitution on atmospheric hydrogen–air flame propagation. Int J Hydrog Energy 2004;29(8):867–79.

[13] Muppala SR, Aluri NK, Dinkelacker F, Leipertz A. Development of an algebraic reaction rate closure for the numerical calculation of turbulent premixed methane, ethylene, and propane/air flames for pressures up to 1.0 MPa. Combust Flame 2005;140(4):257–66.

[14] Ashurst WT, Peters N, Smooke M. Numerical simulation of turbulent flame structure with non-unity Lewis number. Combust Sci Technol 1987;53(4–6):339–75.

[15] Haworth D, Poinsot T. Numerical simulations of Lewis number effects in turbulent premixed flames. J Fluid Mech 1992;244(19):405–36.

[16] Rutland C, Trouvé A. Direct simulations of premixed turbulent flames with nonunity lewis numbers. Combust Flame 1993;94(1–2):41–57.

[17] Trouvé A, Poinsot T. The evolution equation for the flame surface density in turbulent premixed combustion. J Fluid Mech 1994;278(1):1–31.

[18] Chakraborty N, Cant R. Influence of Lewis number on curvature effects in turbulent premixed flame propagation in the thin reaction zones regime. Phys Fluids 2005;17(10):1–21.

[19] Han I, Huh KY. Roles of displacement speed on evolution of flame surface density for different turbulent intensities and Lewis numbers in turbulent premixed combustion. Combust Flame 2008;152(1–2):194–205.

[20] Chakraborty N, Cant R. Effects of Lewis number on scalar transport in turbulent premixed flames. Phys Fluids 2009;21(3):1–12.

[21] Chakraborty N, Cant R. Effects of Lewis number on flame surface density transport in turbulent premixed combustion. Combust Flame 2011;158(9):1768–87.

[22] Chakraborty N. Influence of thermal expansion on fluid dynamics of turbulent premixed combustion and its modelling implications. Flow Turbul Combust 2021;106(3):753–848.

[23] Ozel-Erol G, Klein M, Chakraborty N. Lewis number effects on flame speed statistics in spherical turbulent premixed flames. Flow Turbul Combust 2021;106(4):1043–63.

[24] Cheikhravat H, Goulier J, Bentaib A, Meynet N, Chaumeix N, Paillard C-E. Effects of water sprays on flame propagation in hydrogen/air/steam mixtures. Proc Combust Inst 2015;35(3):2715–22.

[25] Xu P, Ji C, Wang S, Cong X, Ma Z, Tang C, et al. Effects of direct water injection on engine performance in a hydrogen (H2)-fueled engine at varied amounts of injected water and water injection timing. Int J Hydrog Energy 2020;45(24):13523–34.

[26] Lazzarini A, Krauss R, Chelliah H, Linteris GT. Extinction conditions of non-premixed flames with fine droplets of water and water/NaOH solutions. Proc Combust Inst 2000;28(2):2939–45.

[27] Zhang P, Zhou Y, Cao X, Gao X, Bi M. Enhancement effects of methane/air explosion caused by water spraying in a sealed vessel. J Loss Prev Process Ind 2014;29:313–8.

[28] Fan L, Chong CT, Tanno K, McGrath D, Zheng Y, Hochgreb S. Measurement of the effect of water droplets on strained laminar flames using two-phase PIV. Proc Combust Inst 2021;38(2):3183–92.

[29] Chakraborty N, Rasool R, Ahmed U, Klein M. Relations between statistics of three-dimensional flame curvature and its two-dimensional counterpart in turbulent premixed flames. Flow Turbul Combust 2022;109(3):791–812.

[30] Ozel-Erol G, Hasslberger J, Chakraborty N, Klein M. Effects of water droplet injection on turbulent premixed flame propagation: a direct numerical simulation investigation. Flow Turbul Combust 2023;110(1):105–23.

[31] Fernández-Tarrazo E, Sánchez AL, Liñán A, Williams FA. A simple one-step chemistry model for partially premixed hydrocarbon combustion. Combust Flame 2006;147(1–2):32–8.

[32] Keil FB, Amzehnhoff M, Ahmed U, Chakraborty N, Klein M. Comparison of flame propagation statistics extracted from direct numerical simulation based on simple and detailed chemistry—Part 1: Fundamental flame turbulence interaction. Energies 2021;14(17):5548.

[33] Keil FB, Amzehnhoff M, Ahmed U, Chakraborty N, Klein M. Comparison of flame propagation statistics based on direct numerical simulation of simple and detailed chemistry. Part 2: Influence of choice of reaction progress variable. Energies 2021;14(18):5695.

[34] Peters N. The turbulent burning velocity for large-scale and small-scale turbulence. J Fluid Mech 1999;384(5):107–32.

[35] Neophytou A, Mastorakos E, Cant R. DNS of spark ignition and edge flame propagation in turbulent droplet-laden mixing layers. Combust Flame 2010;157(6):1071–86.

[36] Neophytou A, Mastorakos E, Cant RS. The internal structure of igniting turbulent sprays as revealed by complex chemistry DNS. Combust Flame 2012;159(2):641–64.

[37] Jin S, Zhang H, Zhao N, Zheng H. Simulations of rotating detonation combustion with in-situ evaporating bi-disperse n-heptane sprays. Fuel 2022;314:123087.

[38] Hasslberger J, Concetti R, Chakraborty N, Klein M. Inertial effects on the interaction of water droplets with turbulent premixed flames: A direct numerical simulation analysis. Proc Combust Inst 2023;39(2):2575–86.

[39] Concetti R, Hasslberger J, Chakraborty N, Klein M. Analysis of water droplet interaction with turbulent premixed and spray flames using carrier phase direct numerical simulations. Combust Sci Technol 2023;195(7):1411–33.

[40] Hasslberger J, Concetti R, Chakraborty N, Klein M. DNS of turbulent spray flame water droplet interaction using an Euler-Lagrange-Lagrange scheme. In: 28th international colloquium on dynamics of explosions and reactive systems. Newcastle University; 2022.

[41] Kuo KK. Principles of combustion. New York, NY: Elsevier Science Pub. Co. Inc.; 1986.

[42] Meneveau C, Poinsot T. Stretching and quenching of flamelets in premixed turbulent combustion. Combust Flame 1991;86(4):311–32.

[43] Mantel T, Borghi R. A new model of premixed wrinkled flame propagation based on a scalar dissipation equation. Combust Flame 1994;96(4):443–57.

[44] Poinsot T, Veynante D. Theoretical and numerical combustion. RT Edwards, Inc.; 2005.

[45] Damköhler G. Der einfluss der turbulenz auf die flammengeschwindigkeit in gasgemischen. Z Elektrochem angewandte physikalische Chem 1940;46(11):601–26.

[46] Chakraborty N, Alwazzan D, Klein M, Cant RS. On the validity of Damköhler's first hypothesis in turbulent bunsen burner flames: A computational analysis. Proc Combust Inst 2019;37(2):2231–9.

[47] Bechtold J, Matalon M. The dependence of the Markstein length on stoichiometry. Combust Flame 2001;127(1–2):1906–13.

[48] Bane S, Ziegler J, Shepherd J. Development of one-step chemistry models for flame and ignition simulation. GALCIT Rep GALTCITFM 2010;2010:53.

[49] Berger L, Grinberg M, Jürgens B, Lapenna PE, Creta F, Attili A, et al. Flame fingers and interactions of hydrodynamic and thermodiffusive instabilities in laminar lean hydrogen flames. Proc Combust Inst 2023;39(2):1525–34.